Array imaging using intensity-only measurements

Anwei Chai

Institute for Computational and Mathematical Engineering, Stanford University, Stanford CA, 94305, USA

E-mail: anwei.chai@gmail.com

Miguel Moscoso

Gregorio Millán Institute, Universidad Carlos III de Madrid, Madrid, 28911, Spain

E-mail: moscoso@math.uc3m.es

George Papanicolaou

Department of Mathematics, Stanford University, Stanford CA, 94305, USA

E-mail: papanicolaou@stanford.edu

Abstract. We introduce a new approach for narrow band array imaging of localized scatterers from intensity-only measurements by considering the possibility of reconstructing the positions and reflectivities of the scatterers exactly from only partial knowledge of the array data, since we assume that phase information is not available. We reformulate this intensity-only imaging problem as a non-convex optimization problem and show that we can have exact recovery by minimizing the rank of a positive semidefinite matrix associated with the unknown reflectivities. Since this optimization problem is NP-hard and is computationally intractable, we replace the rank of the matrix by its nuclear norm, the sum of its singular values, which is a convex programming problem that can be solved in polynomial time. We show that under certain conditions on the array imaging setup and on the scatterer configuration the minimum nuclear norm solution coincides with the minimum rank solution. Numerical experiments explore the robustness of this approach, which recovers sparse reflectivity vectors exactly as solutions of a convex optimization problem.

1. Introduction

In array imaging, we want to determine the location and reflectivities of small or distributed reflectors by sending probing signals from the array and recording the backscattered fields [4, 5, 6]. Several imaging algorithms such as Kirchhoff migration (KM), least square imaging (LSQ), and Multiple Signal Classification (MUSIC) may be used for this purpose. These algorithms use the full data set recorded at the array, which means that in the frequency domain both amplitude and phase can be measured and recorded. Phase information, or arrival time information in the time domain, is essential for many imaging problems. There are many situations, however, in which it is difficult to measure and record the phases of the signals received at the array. This is the case, for example, in single molecule detection with optical sensors [27, 36], as well as in three-dimensional imaging of nanostructures, where a near-field probe scans over a sample [1, 33]. The measurement of the optical phases, particularly in the near field, is notoriously difficult and detectors or array sensors generally record only signal intensities.

There is also considerable interest in sensor array imaging with less expensive sensors. For frequencies above ten gigahertz or so it becomes more difficult to measure the phase of the scattered fields directly. Since intensity-only (or phaseless) measurements are much easier to get, we consider in this paper imaging that uses only the amplitude of the received signals at the array. Intensity-only imaging has been considered recently in two main forms. The first uses phase-retrieval strategies to estimate the phases of the scattered fields from intensities [17, 18, 20]. In diffraction tomography, used for determining the three-dimensional structure of objects from scattering data, Maleki and Devaney [28] consider an iterative phase-retrieval algorithm for estimating the phase of the signals before carrying out a reconstruction with the usual filtered back-propagation algorithm. Gbur and Wolf [19] consider a modified form of diffraction tomography which requires knowledge of the field on two planes beyond the scatterers so as to determine the phases. However, these planes must be spaced at distances smaller than a wavelength, which is often impractical at high frequencies. The second class of methods carries out imaging without estimation of the missing phases [29, 22]. To image the locations of several scatterers, Marengo *et al.* [29] consider an intensity-only, signal-subspace imaging algorithm, which is similar to the MUSIC method in full array imaging. MUSIC is a frequently used algorithm for imaging well-separated scatterers based on the singular value decomposition (SVD) of the array response matrix [32, 26, 23, 13]. Recently, Govyadinov *et al.* [22] have considered a method for nanoscale optical tomography in which they construct an image by minimizing the ℓ_2 norm of the unknown reflectivity using the singular value decomposition.

In this paper we study narrow band (single frequency) array imaging of localized scatterers when only the intensity is recorded at the array. The ambient medium is homogeneous so that wave propagation is fully coherent. This type of imaging is

therefore very different from diffuse optical tomography (see [2] and references contained therein) where wave propagation is incoherent because of strong multiple scattering, which implies that only intensities can be measured. In diffuse optical tomography the objective is to reconstruct the optical properties of tissues from measurements of scattered, near-infrared light. The main challenge is in dealing with the strong multiple scattering of light that gives blurred images.

Motivated by the recent developments in compressed sensing [8], we formulate array imaging of localized scatterers as a non-convex optimization problem by minimizing the rank of a positive semidefinite decision matrix. We seek a matrix solution of minimum complexity (the rank here) that matches the given data, and which in our formulation has always rank one. Since the rank minimization problem is NP-hard we replace it by its nuclear norm of the decision matrix, which makes the problem convex and solvable in polynomial time. Under certain conditions on the array imaging configuration and on the scatterers, which imply the Restricted Isometry Property (see Definition 3.1) and sparsity, we show that the nuclear norm minimization problem has the same solution as the rank minimization problem. We show further that this solution is unique.

The convex optimization formulation with the nuclear norm for imaging localized scatterers from intensity-only measurements is new. We analyze here properties of this imaging method. We show that we can have exact recovery of the positions and reflectivities of the the scatterers, and that the optimization problem selects the scatterer configuration that minimizes the complexity of the solution matrix. This produces higher resolution images. In the analysis we use ideas from low-rank modeling [31], especially for matrix completion [9] and for robust principal component analysis [10, 35]. Similar ideas have been used in different imaging problems with full field data, so that both intensity and phase of the scattered fields are available [3, 11, 12, 15, 24, 25]. In this case the forward problem is a linear vector equation instead of a linear matrix one as in the case of intensity-only data. The questions analyzed involve conditions under which ℓ_1 minimization is the right substitute for ℓ_0 minimization. There is a clear parallel between the two problems, that of ℓ_0 minimization of a vector and rank minimization of a matrix. The ℓ_0 norm of a vector is the number of non-zero entries while the rank of a matrix is the number of non-zero singular values, and the ℓ_1 norm of a vector is the sum of the absolute values of its entries while the nuclear norm of a matrix is the sum of its singular values.

We note that the problem considered here is somewhat different from those for which the main issue is to find classes of images or signals for which perfect reconstructions can be obtained. In our formulation the decision matrix associated with the unknown locations and reflectivities always has rank one. However, the conditions under which the optimization problem has a unique solution involve only a linear operator whose entries are products of Green's functions. We show that the optimization problem for imaging using intensity-only measurements has a unique solution if the aperture of the array is large compared to the wavelength of the probing signal and the scatterers are far apart. Our numerical experiments show that this can be achieved in

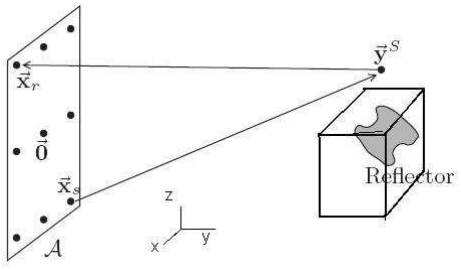

Figure 1. Schematic for array imaging.

practice and that it is robust for noisy data provided that multiple illuminations are used.

The organization of the paper is as follows. We first give a succinct formulation of array imaging in §2. We discuss imaging with full array data and compressed sensing. In §3 we formulate the problem of imaging using intensity-only measurements with rank minimization and give a general condition on linear rank one matrix equation such that rank minimization is equivalent to convex nuclear norm minimization. This ensures that the solution can be obtained in polynomial time. The existence and uniqueness of the unknown reflectivities with intensity-only measurements is proved in §4. Numerical simulations in §5 are carried out to support and extend the theory. The robustness of the imaging method is also studied numerically. We conclude the paper with a brief discussion and possible future work.

2. Problem description

We want to image a small number of localized scatterers or reflectors by sending probing signals from the transducers of an active array and recording the echoes from the scatterers. The setup is shown schematically in Figure 1. The array has N transducers located at $\boldsymbol{x}_p$, for $p = 1, \ldots, N$, separated from each other by h_1. The region around the scatterers to be imaged is the image window (IW), which we assume to be a box $\mathcal{K}$ discretized with a uniform mesh. The K mesh points in the image window are separated by h_2 and denoted by $\boldsymbol{y}_j$, for $j = 1, \ldots, K$. The center of the image window is at a distance L from the center of the array of size $a \times a$.

Within the image window, there are M point scatterers ($M \ll K$) with reflectivities $\rho_j > 0$, for $j = 1, \ldots, M$, and located at unknown locations $\boldsymbol{y}_{n_j}$, $j = 1, \ldots, M$. The number of scatterers is also unknown. We assume that each scatterer is one of the K mesh points in the IW, that is, there are points $\boldsymbol{y}_{n_j}$, $j = 1, \ldots, M$, such that $\{n_1, n_2, \ldots, n_M\} \subset \{1, 2, \ldots, K\}$.

To image the scatterers, we use the *array impulse response matrix* $(\widehat{P}_{pq}(\omega))$, recorded at the array as follows. A signal $\widehat{f}_p(\omega)$ of frequency ω is emitted from transducer p, located at $\boldsymbol{x}_p$, and the back-scattered signals $\widehat{P}_{pq}(\omega)$, received at $\boldsymbol{x}_q$, for $p, q = 1, \ldots, N$, are recorded. The data form the response matrix $\widehat{P}(\omega) = (\widehat{P}_{pq}(\omega))$. For a general

illumination vector $\widehat{\boldsymbol{f}}(\omega) = (\widehat{f}_p(\omega))$, with $\|\widehat{\boldsymbol{f}}(\omega)\|_{\ell_2} = 1$, the data received at the array is given by

$$\widehat{P}(\omega)\widehat{\boldsymbol{f}}(\omega) = \boldsymbol{b}(\omega) \ . \tag{1}$$

The data vector $\boldsymbol{b}(\omega) \in \mathbb{R}^N$ is the response of the scatterers to the illumination vector $\widehat{\boldsymbol{f}}(\omega)$ recorded at the array.

We assume that the scatterers within the image window are well separated so that multiple scattering is negligible. The array response matrix has then the form

$$\widehat{\Pi}(\omega) = (\widehat{\Pi}_{pq}(\omega)) = \sum_{j=1}^{M} \rho_j \widehat{G}_0(\boldsymbol{x}_q, \boldsymbol{y}_{n_j}, \omega)\widehat{G}_0(\boldsymbol{x}_p, \boldsymbol{y}_{n_j}, \omega) \ , \tag{2}$$

where $\widehat{G}_0$ is the Green's function in a homogeneous medium

$$\widehat{G}_0(\boldsymbol{x}, \boldsymbol{y}, \omega) = \frac{e^{i\kappa|\boldsymbol{x}-\boldsymbol{y}|}}{4\pi|\boldsymbol{x}-\boldsymbol{y}|} \ , \quad \kappa = \frac{\omega}{c} \tag{3}$$

with c the propagation speed. We can therefore assume that the array data (1) comes from this model

$$\widehat{\Pi}(\omega)\widehat{\boldsymbol{f}}(\omega) = \boldsymbol{b}(\omega) \ . \tag{4}$$

We introduce the *reflectivity vector* $\boldsymbol{\rho}_0 = (\rho_{01}, \rho_{02}, \ldots, \rho_{0K}) \in \mathbb{R}^K$ such that with the Kronecker delta notation we have

$$\rho_{0k} = \sum_{j=1}^{M} \rho_j \delta_{\boldsymbol{y}_k, \boldsymbol{y}_{n_j}}, \quad k = 1, \ldots, K \, . \tag{5}$$

We also introduce vector of Green's functions

$$\widehat{\boldsymbol{g}}_0(\boldsymbol{y}, \omega) = (\widehat{G}_0(\boldsymbol{x}_1, \boldsymbol{y}, \omega), \widehat{G}_0(\boldsymbol{x}_2, \boldsymbol{y}, \omega), \ldots, \widehat{G}_0(\boldsymbol{x}_N, \boldsymbol{y}, \omega))^T \, , \tag{6}$$

where the superscript T means transpose. We can write $\widehat{\Pi}(\omega)$ in terms of $\widehat{\boldsymbol{g}}_0(\boldsymbol{y}, \omega)$ as

$$\widehat{\Pi}(\omega) = \sum_{j=1}^{M} \rho_j \widehat{\boldsymbol{g}}_0(\boldsymbol{y}_{n_j}, \omega)\widehat{\boldsymbol{g}}_0^T(\boldsymbol{y}_{n_j}, \omega) = \sum_{j=1}^{K} \rho_{0j} \widehat{\boldsymbol{g}}_0(\boldsymbol{y}_j, \omega)\widehat{\boldsymbol{g}}_0^T(\boldsymbol{y}_j, \omega) \, .$$

We now introduce the linear operator $\mathcal{A}_{\widehat{f}(\omega)}$

$$\mathcal{A}_{\widehat{f}(\omega)}\boldsymbol{\rho}_0 = \widehat{\Pi}(\omega)\widehat{\boldsymbol{f}}(\omega) \tag{7}$$

that maps reflectivities $\boldsymbol{\rho}_0$ to array data, with a fixed illumination $\widehat{\boldsymbol{f}}(\omega)$. Using (4), this operator maps the unknown vector $\boldsymbol{\rho}_0$ to the data $\boldsymbol{b}(\omega)$, so that

$$\mathcal{A}_{\widehat{f}(\omega)}\boldsymbol{\rho}_0 = \boldsymbol{b}(\omega) \, . \tag{8}$$

This is the basic equation of array imaging. The data in (8) is complex-valued with both amplitude and phase. In coherent imaging we solve for the unknown reflectivity vector $\boldsymbol{\rho}_0$ from (8), which equates the model with the data. Note that the image window IW is partitioned with a mesh that has a large number of grid points K, while the number of transducers N is limited, and is typically much smaller than K. Therefore (8) is an underdetermined linear system, with fewer measurements than grid points ($N \ll K$).

To get a unique solution for (8) we may look for the minimum ℓ_2 norm solution. In Kirchhoff migration we simply use the adjoint of $\mathcal{A}_{\widehat{f}(\omega)}$ to get an image (see [5] or the appendix in [11] for a quick review).

In the imaging problems considered here we have that $M \ll K$ so the scatterers occupy only a small fraction of the image window IW. This means that the reflectivity vector $\boldsymbol{\rho}_0$ is sparse, so its ℓ_0 norm $\|\boldsymbol{\rho}_0\|_{\ell_0}$ satisfies $\|\boldsymbol{\rho}_0\|_{\ell_0} = M \ll K$. The ℓ_0 norm of a vector is equal to the number of non-zero components. This changes the imaging problem substantially because we can exploit the sparsity of $\boldsymbol{\rho}_0$. We formulate the imaging equation (8) as an optimization problem which seeks the sparsest vector in $\mathbb{R}^K$ that equates model and data. Thus,

$$\min \|\boldsymbol{\rho}\|_{\ell_0} \quad \text{subject to } \mathcal{A}_{\widehat{f}(\omega)}\boldsymbol{\rho} = \boldsymbol{b}(\omega)\,. \tag{9}$$

This problem is, however, non-convex and NP-hard, and so its solution is computationally intractable. To capture the sparsity of $\boldsymbol{\rho}_0$ we use instead the ℓ_1 norm and solve the convex relaxation of (9), which is

$$\min \|\boldsymbol{\rho}\|_{\ell_1} \quad \text{subject to } \mathcal{A}_{\widehat{f}(\omega)}\boldsymbol{\rho} = \boldsymbol{b}(\omega)\,. \tag{10}$$

This can be solved efficiently using linear programming. Donoho [14], Candès and Tao [7] have shown that under certain conditions on $\mathcal{A}_{\widehat{f}(\omega)}$, together with the sparsity of $\boldsymbol{\rho}_0$, problem (10) is equivalent to problem (9). Furthermore, the required minimum number of equations in (8) can be characterized by the sparsity M and the degree of freedom N. This idea is called Basis Pursuit (BP) or Compressed Sensing (CS), under different conditions on $\mathcal{A}_{\widehat{f}(\omega)}$, and has been used in some formulations of array imaging [3, 15, 24, 25]. We have shown in [11, 12] that ℓ_1 minimization can be combined with the singular value decomposition (SVD) so that the reflectivity vector $\boldsymbol{\rho}_0$ can be recovered very efficiently.

3. Imaging using intensity-only measurements

In coherent imaging both amplitude and phase are available. When only the intensity of the data is available, that is, only the absolute value of each entry in $\widehat{\Pi}(\omega)\widehat{\boldsymbol{f}}(\omega)$ is known, the data is given by the vector

$$\boldsymbol{b}_I(\omega) := \operatorname{diag}\Big((\widehat{\Pi}(\omega)\widehat{\boldsymbol{f}}(\omega))(\widehat{\Pi}(\omega)\widehat{\boldsymbol{f}}(\omega))^*\Big)\,, \tag{11}$$

where the superscript $*$ denotes conjugate transpose. In view of the definition (4), the equation for the reflectivity vector $\boldsymbol{\rho}_0$ in intensity-based imaging is given by

$$\operatorname{diag}\left(\mathcal{A}_{\widehat{f}(\omega)}\boldsymbol{\rho}_0\boldsymbol{\rho}_0^*\mathcal{A}_{\widehat{f}(\omega)}^*\right) = \boldsymbol{b}_I(\omega). \tag{12}$$

A straightforward formulation of intensity-based imaging is to compute $\boldsymbol{\rho}_0$ by solving the optimization problem

$$\min \|\boldsymbol{\rho}\|_{\ell_1} \quad \text{subject to } \operatorname{diag}\left(\mathcal{A}_{\widehat{f}(\omega)}\boldsymbol{\rho}\boldsymbol{\rho}^*\mathcal{A}_{\widehat{f}(\omega)}^*\right) = \boldsymbol{b}_I(\omega) \tag{13}$$

analogously to (10) in coherent imaging. However, this problem (13) is neither linear nor convex in $\boldsymbol{\rho}_0$, due to the constraint. Therefore there is no simple algorithm that will give the true global solution effectively.

We reformulate intensity-only imaging as an optimization problem that seeks the sparsest vector in $\mathbb{R}^K$ which equates model and data. We want to solve a linear problem for the unknown sparse reflectivity vector $\boldsymbol{\rho}_0$. To this end, we introduce the matrix decision variable

$$X_0 := \boldsymbol{\rho}_0 \boldsymbol{\rho}_0^* \in \mathbb{R}^{K\times K} ,$$

and the linear map $\mathcal{L}_{\widehat{f}(\omega)} : \mathbb{R}^{K\times K} \to \mathbb{R}^N$ such that $\mathcal{L}_{\widehat{f}(\omega)}(X) := \mathrm{diag}(\mathcal{A}_{\widehat{f}(\omega)} X \mathcal{A}^*_{\widehat{f}(\omega)})$ for any matrix $X \in \mathbb{R}^{K\times K}$. We can now rewrite (12) as

$$\mathcal{L}_{\widehat{f}(\omega)}(X_0) = \boldsymbol{b}_I(\omega) . \tag{14}$$

The reflectivities $\boldsymbol{\rho}_0$ can be obtained by first solving for X_0 from (14) and then taking $\boldsymbol{\rho}_0 = \sqrt{\mathrm{diag}(X_0)}$. Since X_0 is of low rank (of rank 1), sparse (due to the sparsity of $\boldsymbol{\rho}_0$), and real symmetric and positive semidefinite, we may obtain for X_0 from the following rank minimization problem

$$\min \mathrm{rank}(X) \quad \text{subject to } \mathcal{L}_{\widehat{f}(\omega)}(X) = \boldsymbol{b}_I(\omega),\ X \geq 0, \tag{15}$$

where $X \geq 0$ is component-wise non-negativity. Minimizing the rank of a matrix subject to constraints is a general problem that arises in many applications including control, statistics, system identification, etc. ([16] has an overview and many references). However, (15) is a non-convex optimization problem for which the best algorithms require an exponential time in the dimensions of the matrix X. This class of optimization problems is NP-hard, and therefore the exact solution can only be obtained in practice when the dimension of X is very small.

On the basis of convex heuristics we replace $\mathrm{rank}(X)$ in (15) by the nuclear norm $\|X\|_*$ in the objective function. We therefore consider the following optimization problem

$$\min \|X\|_* \quad \text{subject to } \mathcal{L}_{\widehat{f}(\omega)}(X) = \boldsymbol{b}_I(\omega),\ X \geq 0. \tag{16}$$

The nuclear norm $\|\cdot\|_*$ is the sum of the singular values of the matrix while the rank is the number of nonzero singular values. Problem (16) is now convex and can be solved in polynomial time. Since X_0 is formed by an outer product of a vector and its conjugate transpose, it is also positive semidefinite. Under this additional condition, the nuclear norm is the same as the trace. Therefore, the relaxed formulation (16) is equivalent to the trace minimization problem

$$\min \mathrm{trace}(X) \quad \text{subject to } \mathcal{L}_{\widehat{f}(\omega)}(X) = \boldsymbol{b}_I(\omega),\ X \succeq 0,\ X \geq 0, \tag{17}$$

that is often used by the control community [30]. In (17), the symbol $\succeq 0$ stands for positive semidefinite. Both (16) and (17) fall into the category of semi-definite programming (SDP) and can be solved by general purpose solvers.

In general, the two problems (16) (or (17)) are not equivalent to (15). Therefore we must find conditions on the linear operator $\mathcal{L}_{\widehat{f}(\omega)}$ so that the nuclear norm minimization

yields the minimum-rank solution. The solution of these two problems is also not unique, in general. The main contribution of this paper is to show that under certain configurations of the imaging problem, the convex relaxation (16) has the same solution as the non-convex problem (15), and that solution is unique.

When the linear operator $\mathcal{L}_{\widehat{f}(\omega)}$ has the restricted isometry property below, which holds in certain imaging regimes, then (15) has a unique solution which is the same as that of (16). This result is general and holds for any rank minimization problem. We first recall the definition of the restricted isometry constants, widely used in compressed sensing.

Definition 3.1 (Restricted Isometry Property)**.** *Let $\Xi : \mathbb{R}^{m\times n} \to \mathbb{R}^p$ be a linear operator. Assume, without loss of generality, $m \leq n$. For every $1 \leq r \leq m$, define the r-restricted isometry constant to be the smallest number δ_r depending on Ξ such that*

$$(1-\delta_r)\|X\|_F \leq \|\Xi(X)\|_{\ell_2} \leq (1+\delta_r)\|X\|_F$$

holds for all matrices X of rank at most r, where $\|X\|_F = \sqrt{trace(X^*X)} = (\sum_{i=1}^r \sigma_i^2)^{1/2}$ is the Frobenius norm of X, and σ_i denotes its i^{th} largest singular value.

The importance of the Restricted Isometry Property for sparse vectors was realized and exploited by Candès and Tao [7]. It was generalized by Recht, Fazel, and Parrilo to matrices [31]. The constants in the restricted isometry quantify the near-orthogonal behavior of the linear operator Ξ when it is restricted to the sub-variety of matrices of rank at most r. Using this property, we now state the following two low-rank recovery theorems proved in [31].

Theorem 3.2. *Let $\boldsymbol{c} = \Xi(X_0)$ and suppose $\delta_{2r} < 1$ for some integer $r = rank(X_0) \geq 1$. Then X_0 is the only matrix of rank at most r satisfying the matrix equation $\Xi(X) = \boldsymbol{c}$.*

In other words, Theorem 3.2 implies that as long as $\delta_{2r} < 1$, the rank minimization problem

$$\min \operatorname{rank}(X) \quad \text{subject to } \Xi(X) = \boldsymbol{c} \tag{18}$$

has a unique solution which is equal to the exact solution X_0. The next theorem gives an ℓ_1-type recovery result.

Theorem 3.3. *Suppose $r = rank(X_0) \geq 1$ and $\delta_{5r} < 1/10$. Then, X_0 is the unique solution to*

$$\min \|X\|_* \quad \textit{subject to } \Xi(X) = \boldsymbol{c}. \tag{19}$$

Note that by the definition of the restricted isometry constants δ_r, we know that $\delta_r \leq \delta_{r'}$ if $r \leq r'$. Therefore the condition in Theorem 3.3 implies that $\delta_{2r} \leq \delta_{5r} < 1/10 < 1$, and as long as $\delta_{5r} < 1/10$ the solution to (18) is also unique and equal to X_0. In other words, if $\delta_{5r} < 1/10$ the rank minimization problem (18) and the nuclear norm heuristic (19) are equivalent. This result holds for any r. However, when $r = 1$, that is, when the rank of X_0 is one, the restricted isometry condition $\delta_{5r} < 1/10$ can be improved. We prove next the following theorem.

Theorem 3.4. *Let $\boldsymbol{c} = \Xi(X_0)$ with rank$(X_0) = 1$. Assume that $\delta_2 < 1$. Then X_0 is the unique solution to the nuclear norm heuristic (19).*

Proof. Suppose that the solution to (19) has rank greater than 1. Assume X is one such solution to (19). Then we have that

$$\frac{\|X\|_*}{\|X\|} > 1$$

where $\|\cdot\|$ is the operator norm of a matrix, which is equal to its largest singular value σ_1. On the other hand, we know that

$$\frac{\|X\|_*}{\|X\|} \leq \operatorname{rank}(X). \tag{20}$$

Since $\delta_2 < 1$, Theorem 3.2 implies that X_0 is the unique solution to (18). Taking the minimum over the whole solution set of matrices to (19) satisfying $\Xi(X) = \boldsymbol{c}$ on both sides of (20) we have

$$\min_{\Xi(X)=\boldsymbol{c}} \frac{\|X\|_*}{\|X\|} \leq \min_{\Xi(X)=\boldsymbol{c}} \operatorname{rank}(X) = \operatorname{rank}(X_0) = 1.$$

This is a contradiction. Therefore, the solution to (19) must have rank equal to 1. The uniqueness of (18) implies therefore the uniqueness of (19). This concludes the proof. □

4. Main result

In our formulation of the imaging problem with intensity-only measurements the linear operator is given by $\Xi := \mathcal{L}_{\widehat{f}(\omega)}$ and $\boldsymbol{c} := \boldsymbol{b}_I(\omega)$. Comparing (16) and (19), we note that we have one more constraint, which requires the entries of the decision matrix to be non-negative. This additional constraint restricts the problem to a convex subset of (19). Since (16) is convex, there always exists at least one solution. To show that the solution to (16) is unique, we only need to show that (19) has a unique solution equal to $X_0 = \boldsymbol{\rho}_0 \boldsymbol{\rho}_0^*$. Moreover, since the data $\boldsymbol{b}_I(\omega)$ is related to a rank 1 matrix, we know from Theorem 3.4 that we only need to show $\mathcal{L}_{\widehat{f}(\omega)}$ satisfies that $\delta_2 < 1$. We show in this section that the condition $\delta_2 < 1$ holds for the operator $\mathcal{L}_{\widehat{f}(\omega)}$ under certain conditions on the imaging and scatterer configurations.

We first write out the explicit form of $\mathcal{L}_{\widehat{f}(\omega)}$. For any matrix X, the n^{th} entry of the vector $\mathcal{L}_{\widehat{f}(\omega)}(X)$, $n = 1, \ldots, N$, is given by

$$\begin{aligned}
\Big(\mathcal{L}_{\widehat{f}(\omega)}(X)\Big)_n &= \Big(\operatorname{diag}(\mathcal{A}_{\widehat{f}(\omega)} X \mathcal{A}^*_{\widehat{f}(\omega)})\Big)_n = \Big(\mathcal{A}_{\widehat{f}(\omega)} X \mathcal{A}^*_{\widehat{f}(\omega)}\Big)_{nn} = \sum_{k=1}^{K} (\mathcal{A}_{\widehat{f}(\omega)} X)_{nk} (\mathcal{A}^*_{\widehat{f}(\omega)})_{kn} \\
&= \sum_{k=1}^{K} \Big(\sum_{\ell=1}^{K} (\widehat{\boldsymbol{g}}_0^T(\boldsymbol{y}_\ell, \omega) \widehat{f}(\omega)) \widehat{G}_0(\boldsymbol{x}_n, \boldsymbol{y}_\ell, \omega) X_{\ell k} \Big) \overline{(\widehat{\boldsymbol{g}}_0^T(\boldsymbol{y}_k, \omega) \widehat{f}(\omega)) \widehat{G}_0(\boldsymbol{x}_n, \boldsymbol{y}_k, \omega)} \\
&= \sum_{k,\ell=1}^{K} (\widehat{\boldsymbol{g}}_0^T(\boldsymbol{y}_\ell, \omega) \widehat{f}(\omega)) \overline{(\widehat{\boldsymbol{g}}_0^T(\boldsymbol{y}_k) \widehat{f}(\omega))} \widehat{G}_0(\boldsymbol{x}_n, \boldsymbol{y}_\ell, \omega) \overline{\widehat{G}_0(\boldsymbol{x}_n, \boldsymbol{y}_k, \omega)} X_{\ell k}.
\end{aligned}$$

To evaluate δ_2 for $\mathcal{L}_{\widehat{f}(\omega)}$, we need the following Lemma that gives estimates of the sum of products of four Green functions.

Lemma 4.1. *Consider a planar array of size $a\times a$ illuminating an image window that is at a distance L from it. Let $\boldsymbol{y}_{k_i}$, $\boldsymbol{y}_{\ell_i}$, $i=1,2$ be four grid points within the image window, and $\boldsymbol{x}_n$, $n=1,\ldots,N$, the positions of the transducers on the array. If $L\gg a\gg\lambda_0$, where λ_0 is the wavelength, then we have the following results:*

R1 *If $k_1\neq k_2$ or $\ell_1\neq\ell_2$,*

$$\sum_{n=1}^{N}\widehat{G}_0(\boldsymbol{x}_n,\boldsymbol{y}_{k_1},\omega)\overline{\widehat{G}_0(\boldsymbol{x}_n,\boldsymbol{y}_{k_2},\omega)}\widehat{G}_0(\boldsymbol{x}_n,\boldsymbol{y}_{\ell_1},\omega)\overline{\widehat{G}_0(\boldsymbol{x}_n,\boldsymbol{y}_{\ell_2},\omega)}\approx 0. \tag{21}$$

R2 *If $k_1=k_2=k$, $\ell_1=\ell_2=\ell$, and $k\neq\ell$, with $\eta=|\boldsymbol{y}_k-\boldsymbol{y}_\ell|$,*

$$\begin{aligned}
&\frac{1}{2}\frac{2\pi}{(4\pi)^4h_1^2}\frac{\log\left(1+\frac{\eta^2}{L^2}\right)\eta L+2\eta^2\arctan\left(\frac{\eta}{L}\right)+4L^2\arctan\left(\frac{\eta}{L}\right)-\eta\pi}{\eta L(\eta^2+4L^2)}\\
&\lesssim\sum_{n=1}^{N}|\widehat{G}_0(\boldsymbol{x}_n,\boldsymbol{y}_k,\omega)|^2|\widehat{G}_0(\boldsymbol{x}_n,\boldsymbol{y}_\ell,\omega)|^2 \qquad (22)\\
&\lesssim\frac{1}{2}\frac{2\pi}{(4\pi)^4h_1^2}\frac{\log\left(1+\frac{\eta^2}{L^2}\right)\eta L+2\eta^2\arctan\left(\frac{\eta}{L}\right)+4L^2\arctan\left(\frac{\eta}{L}\right)+\eta\pi}{\eta L(\eta^2+4L^2)}.
\end{aligned}$$

R3 *If $k_1=k_2=\ell_1=\ell_2=\ell$,*

$$\sum_{n=1}^{N}|\widehat{G}_0(\boldsymbol{x}_n,\boldsymbol{y}_\ell,\omega)|^4\approx\frac{1}{2}\frac{2\pi}{(4\pi)^4h_1^2L^2}. \tag{23}$$

Proof. We recall that our imaging configuration consists of a planar array with N transducers located at $\boldsymbol{x}_n$ and separated from each other by a distance h_1. The image window is discretized with a uniform mesh of grid size h_2. The cross range resolution is, in the present context, $\lambda_0 L/a$ [5]. Therefore, since $L\gg a$, if $h_2=\lambda_0 L/a$ we have that $h_2\gg\lambda_0$.

Under the large array asymptotic condition ($a\gg\lambda_0$ and $h_1\ll a$) we can replace the sum of the products of the four Green functions by its continuum limit. Hence,

$$\begin{aligned}
&\sum_{n=1}^{N}\widehat{G}_0(\boldsymbol{x}_n,\boldsymbol{y}_{k_1},\omega)\overline{\widehat{G}_0(\boldsymbol{x}_n,\boldsymbol{y}_{k_2},\omega)}\widehat{G}_0(\boldsymbol{x}_n,\boldsymbol{y}_{\ell_1},\omega)\overline{\widehat{G}_0(\boldsymbol{x}_n,\boldsymbol{y}_{\ell_2},\omega)}\approx\\
&\frac{1}{(4\pi)^4h_1^2}\int_{\Omega(\boldsymbol{x})}\frac{\mathrm{e}^{i\kappa(|\boldsymbol{x}-\boldsymbol{y}_{k_1}|-|\boldsymbol{x}-\boldsymbol{y}_{k_2}|)}}{|\boldsymbol{x}-\boldsymbol{y}_{k_1}||\boldsymbol{x}-\boldsymbol{y}_{k_2}|}\frac{\mathrm{e}^{i\kappa(|\boldsymbol{x}-\boldsymbol{y}_{\ell_1}|-|\boldsymbol{x}-\boldsymbol{y}_{\ell_2}|)}}{|\boldsymbol{x}-\boldsymbol{y}_{\ell_1}||\boldsymbol{x}-\boldsymbol{y}_{\ell_2}|}\,\mathrm{d}\boldsymbol{x},
\end{aligned}$$

where $\Omega(\boldsymbol{x})$ is the integral region over the entire array.

R1 Note that when $k_1\neq k_2$ or $\ell_1\neq\ell_2$, the condition $h_2\gg\lambda_0$ implies that the exponents in the integrand are much bigger than 1. Therefore the exponential varies rapidly and the contributions from each $\mathrm{d}\boldsymbol{x}$ to the integral cancel each other, so the net result is negligible. Its leading term behavior is obtained using

the *stationary phase method*. For simplicity, denote the integral by $\mathcal{I}$, and let $\Phi(\boldsymbol{x}) = |\boldsymbol{x}-\boldsymbol{y}_{k_1}| - |\boldsymbol{x}-\boldsymbol{y}_{k_2}| + |\boldsymbol{x}-\boldsymbol{y}_{\ell_1}| - |\boldsymbol{x}-\boldsymbol{y}_{\ell_2}|$. To find the stationary point, we compute the gradient of $\Phi(\boldsymbol{x})$ as

$$\nabla\Phi(\boldsymbol{x}) = \frac{\boldsymbol{x}-\boldsymbol{y}_{k_1}}{|\boldsymbol{x}-\boldsymbol{y}_{k_1}|} - \frac{\boldsymbol{x}-\boldsymbol{y}_{k_2}}{|\boldsymbol{x}-\boldsymbol{y}_{k_2}|} + \frac{\boldsymbol{x}-\boldsymbol{y}_{\ell_1}}{|\boldsymbol{x}-\boldsymbol{y}_{\ell_1}|} - \frac{\boldsymbol{x}-\boldsymbol{y}_{\ell_2}}{|\boldsymbol{x}-\boldsymbol{y}_{\ell_2}|}.$$

This gradient is equal to zero when the four unit vectors are linearly dependent. When k_1, k_2, ℓ_1, and ℓ_2 are not identical, the set of points $\boldsymbol{x}$ that make four unit vectors linearly dependent is finite. Without loss of generality, in the following we assume there exists only one point $\boldsymbol{x}_0$ such that $\nabla\Phi(\boldsymbol{x}_0) = 0$. Since $\Phi(\boldsymbol{x}_0) \sim O(h_2)$ and $\lambda_0 \ll h_2$, we have that $k\Phi(\boldsymbol{x}_0) \gg 1$. From the stationary phase approximation we have

$$\mathcal{I} \approx \frac{\mathrm{e}^{i\kappa\Phi(\boldsymbol{x}_0)}}{|\boldsymbol{x}_0-\boldsymbol{y}_{k_1}||\boldsymbol{x}_0-\boldsymbol{y}_{k_2}||\boldsymbol{x}_0-\boldsymbol{y}_{\ell_1}||\boldsymbol{x}_0-\boldsymbol{y}_{\ell_2}|} \int_{B(\boldsymbol{x}_0,\varepsilon)} \mathrm{e}^{i\kappa(\boldsymbol{x}-\boldsymbol{x}_0)^T\nabla^2\Phi(\boldsymbol{x}_0)(\boldsymbol{x}-\boldsymbol{x}_0)/2}\,\mathrm{d}\boldsymbol{x}$$

where $B(\boldsymbol{x}_0,\varepsilon)$ is a ball centered at $\boldsymbol{x}_0$ with radius ε. Since the integrant oscillates fast outside $B(\boldsymbol{x}_0,\varepsilon)$, we can extend the integral region to $\mathbb{R}^2$, that is,

$$\mathcal{I} \approx \frac{\mathrm{e}^{i\kappa\Phi(\boldsymbol{x}_0)}}{|\boldsymbol{x}_0-\boldsymbol{y}_{k_1}||\boldsymbol{x}_0-\boldsymbol{y}_{k_2}||\boldsymbol{x}_0-\boldsymbol{y}_{\ell_1}||\boldsymbol{x}_0-\boldsymbol{y}_{\ell_2}|} \int_{\mathbb{R}^2} \mathrm{e}^{i\kappa(\boldsymbol{x}-\boldsymbol{x}_0)^T\nabla^2\Phi(\boldsymbol{x}_0)(\boldsymbol{x}-\boldsymbol{x}_0)/2}\,\mathrm{d}\boldsymbol{x}.$$

The integral is of Frensel type and we can calculate the value of $\mathcal{I}$ as

$$\mathcal{I} \approx \frac{\mathrm{e}^{i\kappa\Phi(\boldsymbol{x}_0)}}{|\boldsymbol{x}_0-\boldsymbol{y}_{k_1}||\boldsymbol{x}_0-\boldsymbol{y}_{k_2}||\boldsymbol{x}_0-\boldsymbol{y}_{\ell_1}||\boldsymbol{x}_0-\boldsymbol{y}_{\ell_2}|} \left(\frac{\pi(1+i)}{\kappa|\nabla^2\Phi(\boldsymbol{x}_0)|}\right).$$

Clearly, $\mathcal{I}$ tends to zero like $1/(\kappa h_2)$.

R2 When $k_1 = k_2 = k$, $\ell_1 = \ell_2 = \ell$, and $k \neq \ell$, the sum is reduced to

$$\sum_{n=1}^{N} |\widehat{G}_0(\boldsymbol{x}_n,\boldsymbol{y}_k,\omega)|^2 |\widehat{G}_0(\boldsymbol{x}_n,\boldsymbol{y}_\ell,\omega)|^2 \approx \frac{1}{(4\pi)^4 h_1^2} \int_{\Omega(\boldsymbol{x})} \frac{1}{|\boldsymbol{x}-\boldsymbol{y}_\ell|^2} \frac{1}{|\boldsymbol{x}-\boldsymbol{y}_k|^2} \mathrm{d}\boldsymbol{x}.$$

To analyze the integral, we set $\boldsymbol{y}_k = (0, L, 0)$ and $\boldsymbol{y}_\ell = (0, L, \eta)$ so that they are on the same slice parallel to the imaging array, and $\eta = |\boldsymbol{y}_k - \boldsymbol{y}_\ell|$. Using the same approach as in [11], the integral is analyzed in spherical coordinates with the transformation

$$\frac{\boldsymbol{x}-\boldsymbol{y}_k}{|\boldsymbol{x}-\boldsymbol{y}_k|} = (\cos\theta\sin\phi, \sin\theta\sin\phi, -\cos\phi).$$

The Jacobian for this change of coordinates is $-L^2\sec^2\phi\tan\phi$, $|\boldsymbol{x}-\boldsymbol{y}_k| = L\sec\phi$, and

$$|\boldsymbol{x}-\boldsymbol{y}_\ell|^2 = L^2\sec^2\phi + \eta^2 - 2\eta L\tan\phi\cos\theta.$$

We can now calculate an asymptotic upper bound of the sum as the size of array becomes large

$$\sum_{n=1}^{N} |\widehat{G}_0(\boldsymbol{x}_n,\boldsymbol{y}_k,\omega)|^2 |\widehat{G}_0(\boldsymbol{x}_n,\boldsymbol{y}_\ell,\omega)|^2$$
$$\approx \frac{1}{(4\pi)^4 h_1^2} \int_{\Omega(\boldsymbol{x})} \frac{1}{|\boldsymbol{x}-\boldsymbol{y}_\ell|^2} \frac{1}{|\boldsymbol{x}-\boldsymbol{y}_k|^2} \mathrm{d}\boldsymbol{x}$$

$$
\begin{aligned}
&= \frac{1}{(4\pi)^4 h_1^2} \int_{\Omega(\theta,\phi)} \frac{\tan\phi}{L^2\sec^2\phi + \eta^2 - 2\eta L\tan\phi\cos\theta} \mathrm{d}\theta\mathrm{d}\phi \\
&\lesssim \frac{2\pi}{(4\pi)^4 h_1^2} \int_0^{\pi/2} \frac{\tan\phi}{L^2\sec^2\phi + \eta^2 - 2\eta L\tan\phi} \mathrm{d}\phi \\
&= \frac{1}{2}\frac{2\pi}{(4\pi)^4 h_1^2} \frac{\log\left(1+\frac{\eta^2}{L^2}\right)\eta L + 2\eta^2 \arctan\left(\frac{\eta}{L}\right) + 4L^2\arctan\left(\frac{\eta}{L}\right) + \eta\pi}{\eta L(\eta^2+4L^2)}.
\end{aligned}
$$

An asymptotic lower bound follows similarly.

R3 The asymptotic value for the integral when $k_1 = k_2 = \ell_1 = \ell_2 = \ell$ is relatively straightforward

$$
\begin{aligned}
\sum_{n=1}^{N} |\widehat{G}_0(\boldsymbol{x}_n, \boldsymbol{y}_\ell)|^4 &\approx \frac{1}{(4\pi)^4 h_1^2} \int_{\Omega(\boldsymbol{x})} \frac{1}{|\boldsymbol{x}-\boldsymbol{y}_\ell|^4} \mathrm{d}\boldsymbol{x} \\
&= \frac{1}{(4\pi)^4 h_1^2} \int_{\Omega(\theta,\phi)} \frac{\tan\phi}{L^2\sec^2\phi} \mathrm{d}\theta\mathrm{d}\phi \\
&\lesssim \frac{2\pi}{(4\pi)^4 h_1^2 L^2} \int_0^{\pi/2} \frac{\tan\phi}{\sec^2\phi} \mathrm{d}\phi \\
&= \frac{1}{2}\frac{2\pi}{(4\pi)^4 h_1^2 L^2}.
\end{aligned}
$$

□

When we have $L \gg \eta$, the asymptotical upper and lower bounds of **R2** in Lemma 4.1 are close. This is stated in the following corollary.

Corollary 4.2. *When $L \gg \eta$, we have*

$$
\sum_{n=1}^{N} |\widehat{G}_0(\boldsymbol{x}_n, \boldsymbol{y}_k, \omega)|^2 |\widehat{G}_0(\boldsymbol{x}_n, \boldsymbol{y}_\ell, \omega)|^2 \approx \frac{1}{2}\frac{2\pi}{(4\pi)^4 h_1^2 L^2}. \tag{24}
$$

Proof. In the proof of Lemma 4.1, we have

$$
\begin{aligned}
&\sum_{n=1}^{N} |\widehat{G}_0(\boldsymbol{x}_n, \boldsymbol{y}_k, \omega)|^2 |\widehat{G}_0(\boldsymbol{x}_n, \boldsymbol{y}_\ell, \omega)|^2 \\
&\approx \frac{1}{2}\frac{2\pi}{(4\pi)^4 h_1^2} \frac{\log\left(1+\frac{\eta^2}{L^2}\right)\eta L + 2\eta^2\arctan\left(\frac{\eta}{L}\right) + 4L^2\arctan\left(\frac{\eta}{L}\right) \pm \eta^2\pi}{\eta L(\eta^2+4L^2)} \\
&= \frac{1}{2}\frac{2\pi}{(4\pi)^4 h_1^2} \frac{\left(\frac{\eta}{L}\right)^2 \eta L + 2\eta^2\left(\frac{\eta}{L}\right) + 4L^2\left(\frac{\eta}{L}\right) \pm \eta^2\pi + o\left(\frac{\eta^3}{L^3}\right)}{\eta L(\eta^2+4L^2)} \\
&= \frac{1}{2}\frac{2\pi}{(4\pi)^4 h_1^2 L^2} \frac{1 \pm \frac{\pi}{4}\frac{\eta}{L} + \frac{3}{4}\left(\frac{\eta}{L}\right)^2 + o\left(\frac{\eta^3}{L^3}\right)}{1+\frac{1}{4}\frac{\eta^2}{L^2}} \\
&= \frac{1}{2}\frac{2\pi}{(4\pi)^4 h_1^2 L^2} \left(1 \pm \frac{\pi}{4}\frac{\eta}{L} + \frac{1}{2}\left(\frac{\eta}{L}\right)^2 + o\left(\frac{\eta}{L}\right)^3\right).
\end{aligned}
$$

When $L \gg \eta$, we can truncate to the first order and get (24). □

Using Lemma 4.1 and Theorem 3.4, we obtain the *main result* of this paper, which says that the locations and reflectivities of spatially localized or point-like scatterers can be obtained by solving the nuclear norm minimization problem (16).

Theorem 4.3. *Suppose that the conditions in Lemma 4.1 and Corollary 4.2 hold. Then for imaging with intensity-only measurements, solving (16) recovers the exact location and reflectivities of the scatterers.*

Proof. We only need to show $\mathcal{L}_{\widehat{f}(\omega)}$ satisfies RIP with $\delta_2 < 1$ under the given conditions. For any given matrix X using the representation of linear operator $\mathcal{L}_{\widehat{f}(\omega)}$ and Lemma 4.1, we have

$$
\begin{aligned}
&\|\mathcal{L}_{\widehat{f}(\omega)}(X)\|_{\ell_2}^2 \\
&= \sum_{n=1}^{N} \left(\sum_{\ell,k=1}^{K} (\widehat{\boldsymbol{g}}_0^T(\boldsymbol{y}_\ell,\omega)\widehat{\boldsymbol{f}}(\omega))\widehat{G}_0(\boldsymbol{x}_n,\boldsymbol{y}_\ell,\omega)\overline{(\widehat{\boldsymbol{g}}_0^T(\boldsymbol{y}_k,\omega)\widehat{\boldsymbol{f}}(\omega))\widehat{G}_0(\boldsymbol{x}_n,\boldsymbol{y}_k,\omega)} X_{\ell k} \right) \times \\
&\qquad \overline{\left(\sum_{\ell',k'=1}^{K} (\widehat{\boldsymbol{g}}_0^T(\boldsymbol{y}_{\ell'},\omega)\widehat{\boldsymbol{f}}(\omega))\widehat{G}_0(\boldsymbol{x}_n,\boldsymbol{y}_{\ell'},\omega)\overline{(\widehat{\boldsymbol{g}}_0^T(\boldsymbol{y}_{k'},\omega)\widehat{\boldsymbol{f}}(\omega))\widehat{G}_0(\boldsymbol{x}_n,\boldsymbol{y}_{k'},\omega)} X_{\ell' k'} \right)} \\
&= \sum_{\ell,k=1}^{K}\sum_{\ell',k'=1}^{K} (\widehat{\boldsymbol{g}}_0^T(\boldsymbol{y}_\ell,\omega)\widehat{\boldsymbol{f}}(\omega))\overline{(\widehat{\boldsymbol{g}}_0^T(\boldsymbol{y}_{\ell'},\omega)\widehat{\boldsymbol{f}}(\omega))(\widehat{\boldsymbol{g}}_0^T(\boldsymbol{y}_k,\omega)\widehat{\boldsymbol{f}}(\omega))}(\widehat{\boldsymbol{g}}_0^T(\boldsymbol{y}_{k'},\omega)\widehat{\boldsymbol{f}}(\omega)) \times \\
&\qquad \left(\sum_{n=1}^{N} \widehat{G}_0(\boldsymbol{x}_n,\boldsymbol{y}_\ell,\omega)\overline{\widehat{G}_0(\boldsymbol{x}_n,\boldsymbol{y}_{\ell'},\omega)\widehat{G}_0(\boldsymbol{x}_n,\boldsymbol{y}_k,\omega)}\widehat{G}_0(\boldsymbol{x}_n,\boldsymbol{y}_{k'},\omega) \right) X_{\ell k} X_{\ell' k'} \\
&= \sum_{\ell=k,\ell'=k'} |\widehat{\boldsymbol{g}}_0^T(\boldsymbol{y}_\ell,\omega)\widehat{\boldsymbol{f}}(\omega)|^2 |\widehat{\boldsymbol{g}}_0^T(\boldsymbol{y}_{\ell'},\omega)\widehat{\boldsymbol{f}}(\omega)|^2 \left(\sum_{n=1}^{N} |\widehat{G}_0(\boldsymbol{x}_n,\boldsymbol{y}_\ell,\omega)|^2 |\widehat{G}_0(\boldsymbol{x}_n,\boldsymbol{y}_{\ell'},\omega)|^2 \right) X_{\ell\ell} X_{\ell'\ell'} \\
&\quad + \sum_{\ell=\ell',k=k'} |\widehat{\boldsymbol{g}}_0^T(\boldsymbol{y}_\ell,\omega)\widehat{\boldsymbol{f}}(\omega)|^2 |\widehat{\boldsymbol{g}}_0^T(\boldsymbol{y}_k,\omega)\widehat{\boldsymbol{f}}(\omega)|^2 \left(\sum_{n=1}^{N} |\widehat{G}_0(\boldsymbol{x}_n,\boldsymbol{y}_\ell,\omega)|^2 |\widehat{G}_0(\boldsymbol{x}_n,\boldsymbol{y}_k,\omega)|^2 \right) X_{\ell k}^2 \\
&\quad - \sum_{\ell=\ell'=k=k'} |\widehat{\boldsymbol{g}}_0^T(\boldsymbol{y}_\ell,\omega)\widehat{\boldsymbol{f}}(\omega)|^4 \left(\sum_{n=-N}^{N} |\widehat{G}_0(\boldsymbol{x}_n,\boldsymbol{y}_\ell,\omega)|^4 \right) X_{\ell\ell}^2 \\
&= \sum_{k,\ell=1}^{K} |\widehat{\boldsymbol{g}}_0^T(\boldsymbol{y}_k,\omega)\widehat{\boldsymbol{f}}(\omega)|^2 |\widehat{\boldsymbol{g}}_0^T(\boldsymbol{y}_\ell,\omega)\widehat{\boldsymbol{f}}(\omega)|^2 \left(\sum_{n=1}^{N} |\widehat{G}_0(\boldsymbol{x}_n,\boldsymbol{y}_k,\omega)|^2 |\widehat{G}_0(\boldsymbol{x}_n,\boldsymbol{y}_\ell,\omega)|^2 \right) (X_{k\ell}^2 + X_{kk}X_{\ell\ell}) \\
&\quad - \sum_{\ell=\ell'=k=k'} |\widehat{\boldsymbol{g}}_0^T(\boldsymbol{y}_\ell,\omega)\widehat{\boldsymbol{f}}(\omega)|^4 \left(\sum_{n=1}^{N} |\widehat{G}_0(\boldsymbol{x}_n,\boldsymbol{y}_\ell,\omega)|^4 \right) X_{\ell\ell}^2 \\
&\approx \frac{1}{2}\frac{2\pi}{(4\pi)^4 h_1^2 L^2} \left(\sum_{k,\ell=1}^{K} |\widehat{\boldsymbol{g}}_0^T(\boldsymbol{y}_k,\omega)\widehat{\boldsymbol{f}}(\omega)|^2 |\widehat{\boldsymbol{g}}_0^T(\boldsymbol{y}_\ell,\omega)\widehat{\boldsymbol{f}}(\omega)|^2 (X_{k\ell}^2 + X_{kk}X_{\ell\ell}) - \sum_{\ell=1}^{K} |\widehat{\boldsymbol{g}}_0^T(\boldsymbol{y}_\ell,\omega)\widehat{\boldsymbol{f}}(\omega)|^4 X_{\ell\ell}^2 \right).
\end{aligned}
$$

Without loss of generality we consider the case where $\widehat{\boldsymbol{f}}(\omega)$ corresponds to illumination

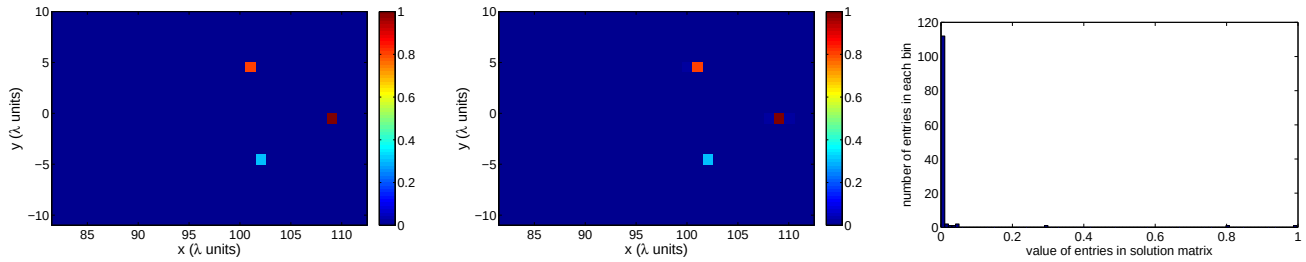

(a) (b) (c)

Figure 2. (a) Original configuration of three scatterers within 10×10 IW where the grid points are separated by 1. (b) Numerical result by solving (17) with no noise in the data and for a single illumination. (c) Histogram of the entries in solution matrix $\tilde{\boldsymbol{\rho}}_0\tilde{\boldsymbol{\rho}}_0^*$. Horizontal axis represents the value range of the entries in $\tilde{\boldsymbol{\rho}}_0\tilde{\boldsymbol{\rho}}_0^*$ using 100 bins. Vertical axis represents the number of entries contained in each bin.

from the center of the array. Then we have that

$$|\widehat{\boldsymbol{g}}_0^T(\boldsymbol{y}_k,\omega)\widehat{\boldsymbol{f}}(\omega)| = \Big|\sum_{n=1}^{N}\widehat{G}_0(\boldsymbol{x}_n,\boldsymbol{y}_k,\omega)\widehat{f}_n(\omega)\Big| = \Big|\frac{1}{4\pi|\boldsymbol{x}_{\lceil N/2\rceil}-\boldsymbol{y}_k|}\Big| \approx \frac{1}{4\pi L}\,,$$

so each multiplier $|\widehat{\boldsymbol{g}}_0^T(\boldsymbol{y}_k,\omega)\widehat{\boldsymbol{f}}(\omega)|^2$ is asymptotically a constant as the size of the array becomes large. Therefore, up to normalization, we have

$$\|\mathcal{L}_{\widehat{f}(\omega)}(X)\|_{\ell_2} \sim \sqrt{\sum_{k,\ell=1}^{K}(X_{k\ell}^2 + X_{kk}X_{\ell\ell}) - \sum_{\ell=1}^{K}X_{\ell\ell}^2} = \sqrt{\|X\|_F^2 + \mathrm{trace}^2(X) - \sum_{\ell=1}^{K}X_{\ell\ell}^2}\,,$$

or

$$\frac{\|\mathcal{L}_{\widehat{f}(\omega)}(X)\|_{\ell_2}}{\|X\|_F} \sim \sqrt{1 + \frac{\mathrm{trace}^2(X) - \sum_{\ell=1}^{K}X_{\ell\ell}^2}{\|X\|_F^2}}.$$

Because $\mathrm{trace}^2(X) \geq \sum_{\ell=1}^{K}X_{\ell\ell}^2$ under $X \geq 0$, we have

$$1 \lesssim \frac{\|\mathcal{L}_{\widehat{f}(\omega)}(X)\|_{\ell_2}}{\|X\|_F} \lesssim \sqrt{1 + \left(\frac{\mathrm{trace}(X)}{\|X\|_F}\right)^2}\,.$$

When $\mathrm{rank}(X) = 1$, $\mathrm{trace}(X) = \|X\|_F$. When $\mathrm{rank}(X) = 2$, $\mathrm{trace}(X) \leq \sqrt{2}\|X\|_F$. Therefore $\delta_2 \leq \max(\sqrt{2}-1, \sqrt{3}-1) < 1$, and the uniqueness of the solution to (16) is proved. □

5. Numerical simulations

In this section we present simulation results that illustrate how the convex optimization formulation of Section 3 performs. The convex programming problem (17) is solved by using the solver SDPT3 [34] with interface provided by the package CVX [21]. We consider simulations in both two and three dimensional space. In the simulations all spatial units are expressed as multiples of λ_0, which is the wavelength of the

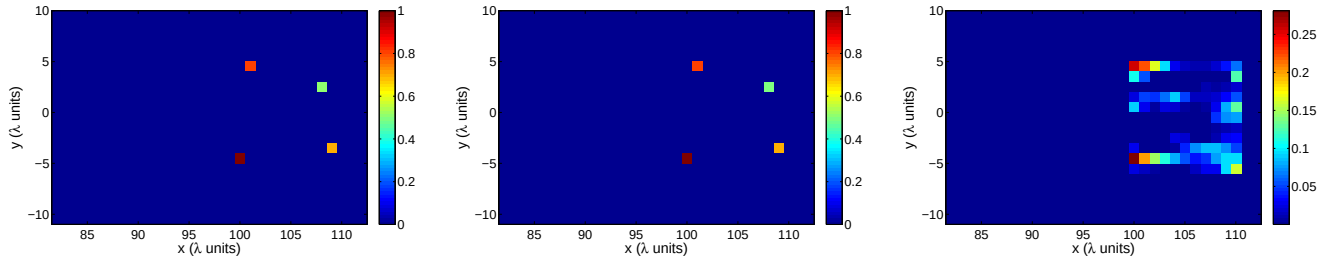

Figure 3. (a) Original configuration of the 10×10 IW with grid points separated by 1. (b) Solution obtained from solving (17) with no noise in the measurements and a single illumination. (c) Solution obtained from solving (26) with 0.5% percent noise in the measurements. The recovered image is blurred and the reflectivity of scatterers is far from the exact values.

illuminating source. Wave propagation between two points $\boldsymbol{x}$, $\boldsymbol{y}$ is calculated using the homogeneous Green's function (3) in three dimensions. For simulations in a two dimensional configuration we still use this Green's function.

We first consider simulations in two dimensions. In the first simulation there are three scatterers of reflectivity 1.0, 0.8 and 0.3, respectively, within an image window of size 10×10 (see Fig. 2 (a)). The image window is at a distance 100 from the linear active array. The array is located on the left and consists of 21 transducers that are 5 wavelengths apart, that is, the aperture is $a = 100$. We put a uniform lattice on the image window with points separated by 1. This results in a 11×11 uniform mesh. There are more points in the image window than transducers in the imaging array.

Figure 2 (b) shows the image obtained using single illumination, that is, $\widehat{f}_q(\omega) = 1$ and $\widehat{f}_p(\omega) = 0$ for $p \neq q$. There is no additive noise in this first example. As we can see, solving (17) recovers the positions of the three scatterers exactly. The values of the recovered reflectivities are 0.9992, 0.7996 and 0.2998, respectively. In Fig. 2 (c) we plot the histogram of the entries of the solution matrix $X_0 = \tilde{\boldsymbol{\rho}}_0 \tilde{\boldsymbol{\rho}}_0^*$, the height of each rectangle being equal to the number of entries with values within the range of the interval. The histogram shows that the recovered matrix is indeed sparse. In fact, except for the 9 largest nonzero entries, the maximal value of the remaining entries is 1.9×10^{-3} .

We now assume that the intensity measured on the array is corrupted by additive noise, so that the equation to invert has the form

$$\operatorname{diag}\left(\mathcal{A}_{\widehat{f}(\omega)} \boldsymbol{\rho}_0 \boldsymbol{\rho}_0^* \mathcal{A}_{\widehat{f}(\omega)}^*\right) = \boldsymbol{b}_I(\omega) + \boldsymbol{e}(\omega). \tag{25}$$

Here, $\boldsymbol{e}(\omega)$ is an unknown noise term. We will assume that its strength is bounded $\|\boldsymbol{e}(\omega)\|_{\ell_2} \leq \varepsilon$, for a fixed constant ε. We solve the following optimization problem

$$\min \|X\|_* \quad \text{subject to } \|\mathcal{L}_{\widehat{f}(\omega)}(X) - \boldsymbol{b}_I(\omega)\|_{\ell_2} \leq \varepsilon,\ X \geq 0\,, \tag{26}$$

which is still convex and where ε is an upper bound of the noise strength.

Figure 3 shows the solutions recovered using our approach with and without adding noise to the data. In both cases there are four scatterers of reflectivity 1.0, 0.8, 0.7 and

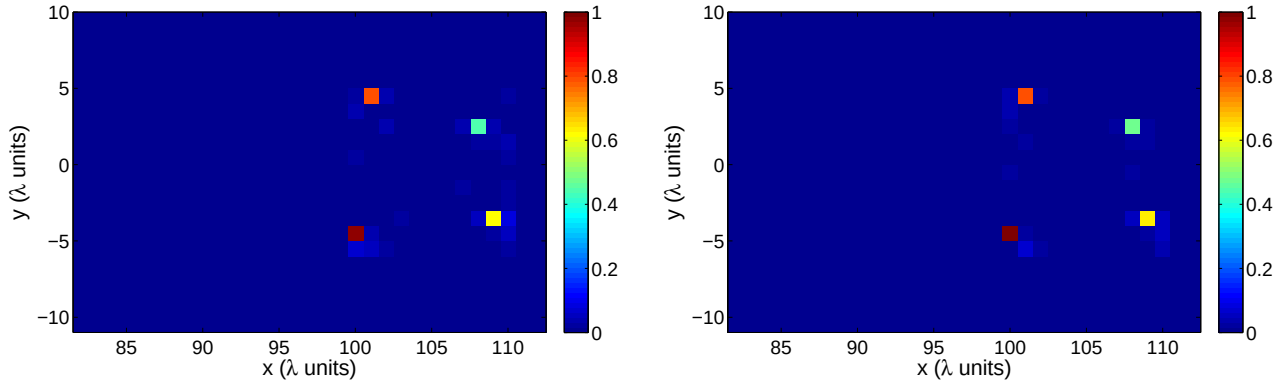

Figure 4. Amount of noise in intensity-only measurement is 0.5%. The number of illuminations is increased to stabilize the solution. (*a*) Solution with 5 different illuminations. (*b*) Solution with 10 different illuminations.

0.5, respectively (see Fig. 3 (a)). The configuration is similar to the previous one (same size of the imaging window, same imaging array, and single illumination). The noise vector $\boldsymbol{e}(\omega)$ is generated by independent Gaussian random variables with zero mean and standard deviation equal to $\alpha\|\boldsymbol{b}_I(\omega)\|_{\ell_2}/\sqrt{N}$. Here, α is used to measure the noise strength. Fig. 3 (b) shows the results when $\alpha = 0$, that is, when there is no noise. The location of the scatterers is recovered exactly while the recovered reflectivities are very close to the real ones. However, when $\alpha = 0.005$, that is, when 0.5% noise is added to the measurements, the location of scatterers gets blurred, as can be seen in Fig. 3 (c).

To compensate for the low resolution seen in Fig. 3 (*c*), we increase the diversity of the illumination sent to the image window. Instead of using a single illumination vector $\widehat{\boldsymbol{f}}(\omega)$ we use multiple illumination vectors $\widehat{\boldsymbol{f}}^{illum}(\omega)$, for $illum = 1, \ldots, Q$, which results in a set of constraints of similar form as the one in (26). For multiple illumination we solve the optimization problem

$$\min \|X\|_* \quad \text{subject to } \|\mathcal{L}_{\widehat{f}^{illum}(\omega)}(X) - \boldsymbol{b}_I^{illum}(\omega)\|_{\ell_2} \leq \varepsilon,\ X \geq 0\,, \qquad (27)$$

for $illum = 1, \ldots, Q$. Figures 4 (a) and (b) show the results when 5 and 10 transducers illuminate the image window, respectively. The configuration is the same as in Fig. 3. It is apparent that the resolution of both images improves a lot. Both recover the correct location of the four scatterers, and when 5 and 10 transducers illuminate the image window, the recovered reflectivities are 0.9790, 0.7865, 0.6209 and 0.4516, and 0.9922, 0.7924, 0.6353 and 0.4731, respectively.

These simulations suggest that constraints of the form $\mathcal{L}_{\widehat{f}(\omega)}(X) = \boldsymbol{b}_I(\omega)$ for the intensity-only imaging problem have very small curvature around the solution, and thus the problem is very sensitive to small perturbations in the data when a single illumination is used. When using more illuminations, and hence adding more constraints in (27), the robustness of the imaging problem improves.

The formulation (26) can handle more noise in the data. Figure 5 shows the results

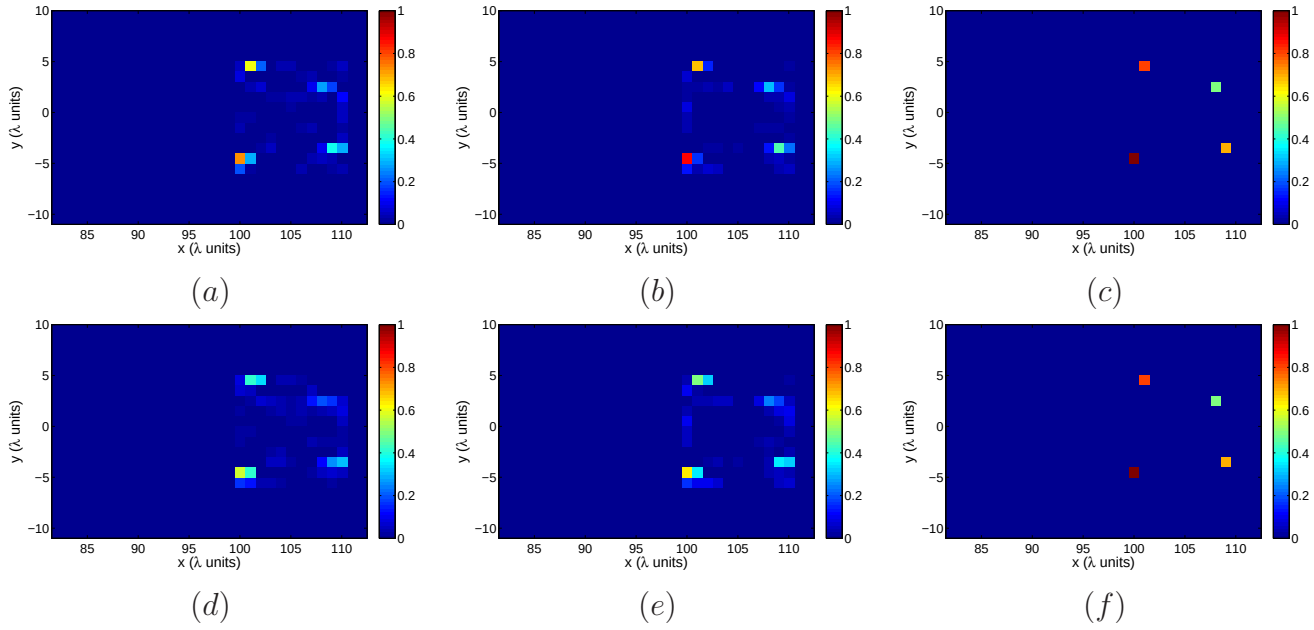

Figure 5. (*a*) 5% noise in intensity-only measurements and 5 illuminations. (*b*) 5% noise in intensity-only measurements and 10 illuminations. (*c*) 5% noise in full measurements and 1 illumination. (*d*) 10% noise in intensity-only measurements and 5 illuminations. (*e*) 10% noise in intensity-only measurements and 10 illuminations. (*f*) 10% noise in full measurements and 1 illumination.

with 5% and 10% noise added to the measurements. We also compare the images with those obtained by solving the ℓ_1 minimization with full measurements, that is, when both intensity and phase are available. As can be seen from the figures, imaging is much more robust to noise when the phases in the measurements are provided.

Finally, in Fig. 6 we show a simulation in 3 dimensions. The location of the scatterers in the image window is shown in the Fig. 6. We use a square array on the xz plane whose dimensions are 10×10. The transducers are placed on a uniform 11×11 grid so that $N = 121$. The image window is a box $\mathcal{K}$, each side of which is 4. The box is at range $L = 100$ and a $5 \times 5 \times 5$ grid is placed uniformly in $\mathcal{K}$. The number of scatterers in $\mathcal{K}$ is $M = 2$ and their reflectivities are 1.0 and 0.8. With this configuration we have a decision matrix X with 5^6 unknowns. Solving (17) we recover the location and reflectivity of the two scatterers very well (see Fig. 6 (a)). The histogram of the solution matrix X_0 is shown in Fig. 6 (c).

6. Conclusion

We consider array imaging of localized scatterers in a homogeneous medium with intensity-only measurements. We analyze situations in which it is possible to reconstruct exactly the positions and reflectivities of the scatterers from this partial knowledge of the data, since phase information is not available. We formulate this imaging problem as finding the minimum rank solution of a linear matrix equation associated with the

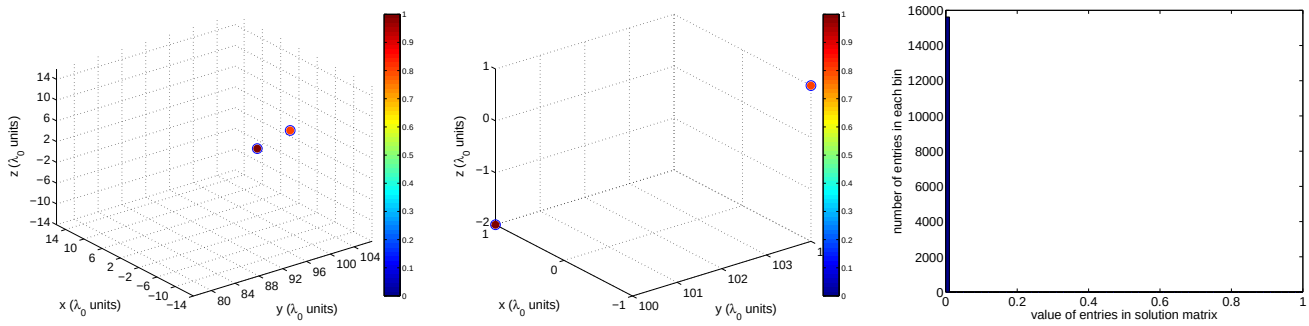

Figure 6. (a) Two scatterers are placed far apart within $4 \times 4 \times 4$ box. The location and reflectivity are recovered by solving (17). Solid points represent the solution with color indicating the reflectivity. The circles are the true locations of scatterers which is the same as the solution. The recovered reflectivity is 0.9898 and 0.8078. (b) Zoom-in configuration of the scatterers in image window. (c) Histogram of the solution matrix.

locations and reflectivities of the scatterers. We seek therefore a matrix solution of minimal complexity that matches the intensity data. To find it we use the nuclear norm heuristic and prove that in certain regimes it recovers the locations and reflectivities of the scatterers exactly. This is confirmed with numerical simulations. We also show numerically that this intensity-only array imaging is robust to noise. The theoretical justification of this robustness is an ongoing research effort.

Acknowledgement

This work was partially supported by AFOSR grant FA9550-08-1-0089. AC was supported by a Hewlett-Packard Stanford Graduate Fellowship. MM acknowledges support from the Spanish Ministry of Education and Science (grant FIS2007-62673).

References

[1] Anderson N, Anger P, Hartschuh A and Novotny L 2006 Subsurface raman imaging with nanoscale resolution *Nano Lett.* **6(4)** 744–749

[2] Arridge S R 1999 Optical tomography in medical imaging *Inverse Problems* **15** 41–93

[3] Baraniuk R and Steeghs P 2007 Compressive radar imaging *IEEE Radar Conference* 128-133

[4] Borcea L, Papanicolaou G, Tsogka C and Berryman J 2002 Imaging and time reversal in random media *Inverse Problems* **18** 1247–1279

[5] Borcea L, Papanicolaou G and Tsogka C 2003 Theory and application of time reversal and interferometric imaging, *Inverse Problems* **19** 139–164

[6] Borcea L, Papanicolaou G and Tsogka C 2005 Interferometric array imaging in clutter *Inverse Problems* **21** 1419–1460

[7] Candès E J and Tao T 2005 Decoding by linear programming *IEEE Trans. Inform. Theory* **51** 4203–4215

[8] Candès E J 2006 Compressive sampling *Proc. Int. Congress of Mathematicians Madrid, Spain* **3** 1433–1452

[9] Candès E J and Recht B 2009 Exact matrix completion via convex optimization *Found. of Comput. Math.,* **9** 717–772
[10] Candès E J, Li X, Ma Y and J. Wright 2010 Robust principal component analysis? *Journal of the ACM* (submitted)
[11] Chai A and Papanicolaou G 2010 Imaging localized scatterers using the singular value decomposition and ℓ_1 optimization *Inverse Problems* (submitted)
[12] Chai A and Papanicolaou G 2010 Study of imaging in random medium using a simple random phase model SIAM Journal on Imaging Sciences (submitted)
[13] Devaney A J, Marengo E A and Gruber F K 2005 Time-reversal-based imaging and inverse scattering of multiply scattering point targets *J. Acoust. Soc. Am.* **118** 3129–3138
[14] Donoho D L 2006 Compressed sensing *IEEE Trans. Inform. Theory* **52(4)** 1289–1306
[15] Fannjiang A, Yan P and Strohmer T 2010 Compressed remote sensing of sparse objects *arXiv:0904.3994*
[16] Fazel M 2002 Matrix rank minimization with applications *Ph.D. Thesis* Stanford University
[17] Fienup J R 1978 Reconstruction of an object from the modulus of its Fourier transform *Opt. Lett.* **3** 27–29
[18] Fineup J R 1982 Phase retrieval algorithms: a comparison *Apl. Opt.* **21** 2758–2769
[19] Gbur G and Wolf E 2002 Diffraction tomography without phase information *Opt. Lett.* **27** 1890–1892
[20] Gerchberg R W and Saxton W O 1972 A practical algorithm for the determination of phase from image and diffraction plane pictures *Optik* **35**, 237–246
[21] Grant M and Boyd S 2010 CVX: Matlab software for disciplined convex programming, version 1.21 `http://cvxr.com/cvx`
[22] Govyadinov A A, Panasyuk G Y and Schotland J C 2009 Phaseless Three-Dimensional Optical Nanoimaging *Phys. Rev. Lett.* **103** 213901
[23] Gruber F K, Marengo E A and Devaney A J 2004 Time-reversal imaging with multiple signal classification considering multiple scattering between the targets *J. Acoust. Soc. Am.* **115** 3042–3047
[24] Gurbuz A, McClellan J and Scott W. Jr 2009 A compressive sensing data acquisition and imaging method for stepped frequency GPRs *IEEE Trans. Signal Processing* **57** 2640–2650
[25] Herman M and Strohmer T 2009 High resolution radar via compressed sensing *IEEE Trans. Signal Processing* **57** 2275–2284
[26] Kirsch A 2002 The MUSIC algorithm and the factorization method in inverse scattering theory for inhomogeneous media *Inverse Probl.* **18** 1025–1040
[27] Levene M J, Korlach J, Turner S W, Foquet M, Craighead H G and Webb W W 2003 Zero-Mode Waveguides for Single-Molecule Analysis at High Concentrations *Science* **299(5607)** 682–699
[28] Maleki M H and Devaney A J 1993 Phase retrieval and intensity-only reconstruction algorithms from optical diffraction tomography *J. Opt. Soc. Am. A* **10** 1086–1092
[29] Marengo E A, Hernandez R D and Lev-Ari H 2007 Intensity-only signal-subspace-based imaging *J. Opt. Soc. Am. A* **24** 3619–3635
[30] Mesbahi M and Papavassilopoulos G P 1997 On the rank minimization problem over a positive semidefinite linear matrix inequality *IEEE Trans. on Automatic Control* **42** 239–243
[31] Recht B, Fazel M and Parrilo P 2010 Guaranteed minimum-rank solutions of linear matrix equations via nuclear norm minimization *SIAM Review* (to appear)
[32] Schmidt R 1986 Multiple emitter location and signal parameter estimation *IEEE Trans. Antennas Propagation* **34** 276–280
[33] Taubner T, Keilmann F and Hillenbrand R 2005 Nanoscale-resolved subsurface imaging by scattering-type near-field optical microscopy *Opt. Express* **13** 8893–8899
[34] Toh K C, Todd M J and Tutuncu R H SDPT3 — a Matlab software package for semidefinite programming. *Optimization Methods and Software,* **11** 545–581.
[35] Wright J, Ganesh A, Rao S and Ma Y 2009 Robust principal component analysis: exact recovery

of corrupted low-rank matrices via convex optimization, *Proc. of the Conf. on Neur. Infor. Proc. Sys. (NIPS)*

[36] Yin D, Deamer D W, Schmidt H, Barber J P and Hawkins A R 2006 Single-molecule detection sensitivity using planar integrated optics on a chip *Opt. Lett.* **31** 2136–2138